RESEARCH ARTICLE OPEN ACCESS

Lifespan Modeling of Choroid Plexus Volume in Multiple Sclerosis and Its Dynamic Associations With Clinical, MRI, and HLA Susceptibility

Paolo Preziosa,[1,2,3] Gianluca Corazzolla,[1,2,3] Alessandro Meani,[1] Monica Margoni,[1,2,4] Loredana Storelli,[1] Elisabetta Pagani,[1] Martina Rubin,[1,2,3] Ferdinando Clarelli,[5] Elisabetta Mascia,[5] Melissa Sorosina,[5] Federica Esposito,[2,5] Massimo Filippi,[1,2,3,4,6] and Maria A. Rocca[1,2,3]

Correspondence
Prof. Rocca
rocca.mara@hsr.it

Neurol Neuroimmunol Neuroinflamm 2026;13:e200593. doi:10.1212/NXI.0000000000200593

Abstract

Background and Objectives

The choroid plexus (ChP) regulates CSF production and CNS homeostasis. In multiple sclerosis (MS), ChP enlargement occurs early in the disease course, yet its normative lifespan trajectory and relationship with MS-specific features remain poorly defined. We aimed to define the normative ChP volume model, to characterize its trajectory across the healthy lifespan, and to assess ChP enlargement in MS using z-scores, evaluating associations with demographic, clinical, MRI, and genetic variables, including human leukocyte antigen (HLA) and non-HLA polygenic risk scores (PRSs).

Methods

This monocentric retrospective cross-sectional study included 461 healthy controls (HCs) and 727 patients with MS (age 18–70 years) who underwent 3T brain MRI and neurologic assessment. ChP volumes were quantified using ASCHOPLEX, normalized for head size, and modeled in HCs. We derived age-related normalized ChP volume (NChPV) trajectory across adulthood. Z-scores for patients with MS were computed. PRSs were calculated from established MS susceptibility loci, encompassing both HLA and non-HLA regions.

Results

In HCs, normalized brain volume, lateral ventricle volume, and its squared term were independently associated with NChPV (R^2 = 0.54). Model-derived NChPV trajectory remained stable until age 35 and then increased nonlinearly (p-FDR<0.002), with annualized growth rates rising from 0.24% at age 35 to over 0.7% in later decades. Patients with MS had significantly higher NChPV z-scores than controls (estimated mean [EM] z-score = 0.452, p-FDR<0.001), consistently across phenotypes (p = 0.744) and ages, with no evidence of age-dependent variation ($\beta = 0.02 \times 10^{-2}$, p = 0.957). In cross-sectional analyses, NChPV z-scores, already elevated 1 year after disease onset (EM z-scores = 0.252, p-FDR<0.001), increased further up to 5 years after disease onset (EM z-scores = 0.463, p-FDR<0.001), before plateauing. Higher z-scores were associated with greater T2-hyperintense white matter lesion volume ($\beta = 0.012 \times 10^{-2}$, $p < 0.001$) and HLA genetic burden (standardized β = 0.097, p = 0.038), but not non-HLA PRSs ($p \geq 0.177$).

Discussion

We provided a normative ChP volume model, characterized its trajectory across the healthy lifespan, and showed early, consistently higher ChP volume in patients with MS across ages and disease durations in cross-sectional analyses, linked to inflammatory lesion burden and HLA-mediated genetic risk. The ChP may represent a noninvasive biomarker of neuroinflammation and HLA-related immunogenetic background in MS.

MORE ONLINE

Supplementary Material

[1]Neuroimaging Research Unit, Division of Neuroscience, IRCCS San Raffaele Scientific Institute, Milan, Italy; [2]Neurology Unit, IRCCS San Raffaele Scientific Institute, Milan, Italy; [3]Vita-Salute San Raffaele University, Milan, Italy; [4]Neurorehabilitation Unit, IRCCS San Raffaele Scientific Institute, Milan, Italy; [5]Laboratory of Human Genetics of Neurological Disorders, IRCCS San Raffaele Scientific Institute, Milan, Italy; and [6]Neurophysiology Service, IRCCS San Raffaele Scientific Institute, Milan, Italy.

The Article Processing Charge was funded by the authors.

Glossary

BCSFB = blood–cerebrospinal fluid barrier; **ChP** = choroid plexus; **DMT** = disease-modifying therapy; **EDSS** = Expanded Disability Status Scale; **ETL** = echo train length; **FLAIR** = fluid-attenuated inversion recovery; **FOV** = field of view; **HC** = healthy control; **HLA** = human leukocyte antigen; **IMSGC** = International Multiple Sclerosis Genetics Consortium; **LV** = lesion volume; **MHC** = major histocompatibility complex; **MS** = multiple sclerosis; **NChPV** = normalized ChP volume; **PP** = primary progressive; **PRS** = polygenic risk score; **RR** = relapsing-remitting; **SP** = secondary progressive; **TE** = echo time; **TR** = repetition time; **WM** = white matter.

Introduction

The CNS is now recognized to undergo active immune surveillance at specialized brain border interfaces.[1] Among these, the choroid plexus (ChP) is a key component of the blood–cerebrospinal fluid barrier (BCSFB) and a major interface between the peripheral immune system and the CNS.[1] Structurally, the ChP consists of epithelial cells connected by tight junctions overlying fenestrated capillaries embedded within loose connective stroma.[1,2] Functionally, it regulates immune cell trafficking between the blood and CSF, acts as a neuroimmune gateway, and produces CSF, contributing to CNS homeostasis.[2]

In multiple sclerosis (MS), a chronic inflammatory, demyelinating, and neurodegenerative disease of the CNS, the ChP accumulates immune cells and may act as an entry point for innate and adaptive immune cells into the CNS.[3,4] MRI-based studies have shown ChP volumetric enlargement since the earliest phases of MS,[5-7] suggesting early ChP involvement in disease pathogenesis. Higher ChP volumes have been associated with more severe structural brain damage, including higher T2-hyperintense white matter (WM) lesion volume (LV), global and regional brain atrophy, and clinical features such as higher relapse rates, more severe disability, cognitive impairment, and fatigue.[5-13]

Recent evidence indicates that ChP volume increases with healthy aging,[14,15] as well as across several neurologic conditions.[4-13,16-21] This enlargement likely reflects age-related morphological[21] and microstructural changes,[22] as well as immune-driven epithelial and stromal remodeling, vascular alterations, and immune cell accumulation.[8] However, although these processes represent plausible biological substrates, the histopathologic determinants of MRI-detected ChP enlargement remain incompletely defined, warranting dedicated histopathologic correlation studies. Given the age-related increase in ChP volume, establishing lifespan-adjusted normative values is essential to distinguish physiologic aging–related variation from MS-related changes. Moreover, because the ChP resides within the ventricular system, its MRI-based volumetric estimation is strongly correlated with brain atrophy and ventricular expansion, as consistently shown in both healthy controls (HCs)[5,12,13] and patients with neurologic diseases.[5,7,9,16,18] This association likely reflects shared morphometric dependencies rather than a direct causal relationship. In addition, ventricular expansion may increase the free CSF surrounding the ChP, thereby improving its visualization and segmentation on MRI and potentially contributing to the apparent ChP enlargement measured in vivo. However, the complex interdependence among ChP volume, age, and brain volumetric measures has not been fully explored.

From a genetic perspective, MS susceptibility is highly polygenic and is predominantly driven by immune-related loci, with the strongest contribution arising from the major histocompatibility complex (MHC) region.[23,24] In particular, the human leukocyte antigen (HLA)-DRB1*15:01 allele represents the most robust and consistently replicated genetic risk factor of MS, supporting the central role of antigen presentation and adaptive immune activation in disease pathogenesis. Beyond the HLA region, several common variants of small effect contribute additively to MS risk, and this cumulative genetic liability can be summarized using polygenic risk scores (PRSs),[23] which reflect genome-wide susceptibility enrichment at different statistical thresholds. PRSs of MS susceptibility have been associated with earlier disease onset[24-27] and higher relapse activity,[27,28] but not with long-term disability or neurodegeneration.[24,26,29] Given the immunologic functions of the ChP at the BCSFB, it is plausible that inherited immune risk may relate to structural variability at this brain-immune interface. Integrating genetic and imaging data may, therefore, clarify whether immunogenetic burden contributes to interindividual variability in ChP volume.

Against this background, we conducted a retrospective cross-sectional study to model normative ChP volume trajectories across the adult lifespan using a large, monocentric cohort of HCs acquired with 2 different 3 Tesla (3T) MRI scanners, while adjusting for key demographic features, brain morphometric parameters, and scanner effects. Using this model, we then computed individualized ChP volume z-scores for patients with MS to quantify deviations from expected normative values based on age, sex, and brain volumetric measures. These z-scores were subsequently used to explore associations with clinical features, MRI metrics of structural brain damage, and immune-related genetic burden. Considering the immunologic functions of the ChP and its early volumetric enlargement in MS, we tested whether human leukocyte antigen (HLA) and non-HLA PRSs[23] were associated with ChP volumetric abnormalities, providing insight

into the immunogenetic contribution to interindividual variability in ChP volume in MS.

Methods

Study Design and Population

From the single-center database of the Neuroimaging Research Unit, IRCCS San Raffaele Scientific Institute (Milan, Italy), we retrospectively selected 727 patients with MS and 461 HCs who underwent the same MRI protocol between July 2005 and October 2024,. Inclusion and exclusion criteria are detailed in eMethods.

Clinical Assessment

Within 3 days of the MRI scan, patients with MS underwent a neurologic examination with Expanded Disability Status Scale (EDSS) scoring and documentation of disease onset date, current disease-modifying therapy (DMT), and clinical phenotype (i.e., relapsing-remitting [RR], secondary progressive [SP], or primary progressive [PP]).

MRI Acquisition

Brain MRI examinations were performed using 2 3.0T scanners (Scanner 1: Achieva, 404 patients with MS and 207 HCs; Scanner 2: Ingenia, 323 patients with MS and 254 HCs; Philips Medical Systems, Eindhoven, the Netherlands). MRI acquisitions for Scanner 1 were conducted between July 2005 and May 2016 and for Scanner 2 between October 2016 and October 2024. During each scanner-specific period, the gradient system and head coil configuration remained stable, and no protocol changes or major hardware/software upgrades were introduced that could systematically affect volumetric measurements.

Images acquired with Scanner 1 included the following: (1) dual-echo turbo spin echo (repetition time [TR] = 2,599; echo time [TE] = 16–80 msec; flip angle = 90°; matrix size = 256 × 256; field of view [FOV] = 240 mm^2; echo train length [ETL] = 6; 44 contiguous axial slices, 3-mm thick) and (2) three-dimensional (3D) T1-weighted fast field echo (TR = 25; TE = 4.6 msec; flip angle = 30°; matrix size = 256 × 256; FOV = 230 mm^2; 220 contiguous axial slices, 0.8-mm thick).

Images acquired with Scanner 2 included the following: (1) 3D T2-weighted fluid-attenuated inversion recovery (FLAIR) (TR = 4,800 msec; TE = 270 msec; inversion time [TI] = 1,650 msec; matrix size = 256 × 256; FOV = 256 × 256 mm^2; ETL = 167; 192 contiguous sagittal slices, 1-mm thick); (2) 3D T2-weighted turbo spin echo (TR = 2,500 msec; TE = 330 msec; matrix size = 256 × 256; FOV = 256 × 256 mm^2; ETL = 117; 192 contiguous sagittal slices, 1-mm thick); and (3) 3D T1-weighted turbo field echo (TR = 7 msec; TE = 3.2 msec; TI = 1,000 msec; flip angle = 8°; matrix size = 256 × 256; FOV = 256 × 256 mm^2; 204 contiguous sagittal slices, 1-mm thick).

Structural MRI Analysis

For both patients with MS and HCs, focal T2-hyperintense WM lesions were quantified using scanner-specific optimized acquisition approaches. For Scanner 1, T2-hyperintense WM lesions were identified on dual-echo TSE images and segmented manually by trained raters (P.P. and M.M.) with >10 years of experience in lesion delineation through a semiautomatic local thresholding segmentation technique (Jim 8.0, Xinapse Systems Ltd, Colchester, UK). For Scanner 2, lesion segmentation was performed using a fully automated pipeline, with 3D FLAIR and 3D T1-weighted images as input. Total brain T2-hyperintense WM LV volume was calculated from the lesion masks after careful visual quality control of the segmentation results by the same raters, with manual editing performed when necessary, and subsequently normalized for head size. Normalized brain (global, cortical, thalamic, and caudate) and lateral ventricle volumes were obtained using FSL-SIENAx and FSL-FIRST after lesion refilling. eMethods provides details.

Automatic Choroid Plexus Segmentation

A fully automatic method to segment ChP on 3D T1-weighted images was implemented using the artificial intelligence–based ASCHOPLEX toolbox[30] (eFigure 1). The toolbox is based on a deep-learning approach composed of 27 deep neural network configurations. After automated segmentation, all ChP masks were visually inspected by expert readers (P.P. and M.M., >15 years of experience in neuroimaging segmentation quality control) and manual intervention was limited to cases strictly necessary to preserve pipeline reproducibility and minimize operator-dependent biases. eMethods provide additional details.

Genotyping, Imputation, and PRS Calculation

Whole-genome genotyping was performed on a larger cohort of patients with MS using multiple Illumina® arrays. Comprehensive quality control, imputation procedures, and platform-specific steps are described in eMethods. PRSs for MS susceptibility were calculated based on established loci identified by the International Multiple Sclerosis Genetics Consortium (IMSGC).[23] Three non-HLA PRSs were computed to represent progressively inclusive sets of risk variants, capturing different levels of statistical evidence. A separate HLA Genetic Burden (HLAGB) score was computed from 24 MS-associated HLA loci.

Statistical Analysis

Lifespan trajectories of normalized brain, cortical, thalamic, caudate, lateral ventricle, and ChP volumes in HCs were estimated from scanner-adjusted robust regression models, with bootstrap-based stepwise term selection. ChP models incorporated brain and ventricular volumes to account for shared anatomical scaling. Brain volumes in patients with MS were converted to z-scores relative to HCs; robust regression tested deviations, phenotype differences, and associations with age, disease duration, disability, T2-hyperintense WM LV, and genetic scores. We controlled for multiple testing

using the false discovery rate (FDR; Benjamini-Hochberg procedure). Sensitivity analyses included modeling on combined HC and MS samples to assess robustness and consistency of z-scores.

p Values < 0.05 were deemed statistically significant. eMethods provide detailed statistical analysis.

Standard Protocol Approvals, Registrations, and Patient Consents

This was a retrospective cross-sectional study. Approval was received from the local institutional ethical standards committee on human experimentation (protocol number 2009-74). Written informed consent was obtained from all participants prior to study participation according to the Declaration of Helsinki.

Data Availability

The corresponding author, who had full access to all study data, assumes responsibility for the integrity of the data and the accuracy of the analysis. The anonymized data set used and analyzed in this study is available on reasonable request from the corresponding author.

Results

Demographic Features and Volumetric Associations in HCs

We included 461 HCs (female = 251 [54%]; mean age = 41.9 [SD = 15.1], range = 18.1; 69.8 years). The 2 scanner subcohorts did not differ in sex ($p = 0.328$) or age ($p = 0.102$) (eTable 1). The overall MS cohort (n = 727) consisted of 477 patients with RRMS, 160 with SPMS, and 90 with PPMS (Table 1). Compared with HCs, patients with MS were more frequently female (61% vs 54%, $p = 0.022$), while age did not differ ($p = 0.373$), with HCs covering the full age range of the MS cohort.

In HCs, higher normalized ChP volume correlated with older age ($r = 0.323$, $p < 0.001$); lower normalized brain volume ($r = -0.453$, $p < 0.001$); and lower cortical ($r = -0.330$, $p < 0.001$), thalamic ($r = -0.280$, $p < 0.001$), and caudate ($r = -0.141$, $p = 0.002$) volumes, as well as with higher lateral ventricle volume ($r = 0.636$, $p < 0.001$). Log-transformed lateral ventricle volume improved distribution symmetry, reduced the influence of extreme values, and strengthened the correlation with ChP volume ($r = 0.713$, $p < 0.001$). No significant sex difference in normalized ChP volume was found ($p = 0.396$).

Normalized brain volume ($\beta = -1.11 \times 10^{-3}$, standard error [SE] = 0.38×10^{-3}, $p = 0.004$), log-transformed normalized lateral ventricle volume ($\beta = 1.74$, SE = 0.10, $p < 0.001$), and its squared term ($\beta = -1.53$, SE = 0.32, $p < 0.001$) were all independently associated with normalized ChP volume in a scanner-adjusted multivariable model ($R^2 = 0.54$). Age was not retained in this final model. For comparison, a model based only on demographic variables retained age ($\beta = 1.00 \times 10^{-2}$, SE = 0.15×10^{-2}, $p < 0.001$) and age squared ($\beta = 0.44 \times 10^{-3}$, SE = 0.12×10^{-3}, $p < 0.001$) but explained substantially less variance ($R^2 = 0.16$).

Volumetric Trajectories in HCs Across the Adult Lifespan

Different age-related volumetric trajectories were observed across the brain structures in HCs (Table 2, Figure 1).

Normalized brain and thalamic volumes followed quadratic decreasing patterns (brain: $\beta = -3.16 \times 10^{-2}$, SE = 1.05×10^{-2}, $p = 0.003$; thalamus: $\beta = -1.07 \times 10^{-3}$, SE = 0.37×10^{-3}, $p = 0.004$), with significant volume decline emerging around ages 30 and 35, respectively (all p-FDR<0.004), and progressively accelerating annual reduction rates (brain: from −0.08% to −0.25%; thalamus: from −0.08% to −0.44%).

Normalized lateral ventricle volumes exhibited a quadratic increase on log scale ($\beta = 1.56 \times 10^{-4}$, SE = 0.44×10^{-4}, $p < 0.001$), with a positive slope, reflecting enlargement, emerging at approximately 35 years (all p-FDR<0.007) and annual expansion rising from approximately 0.4% at age 35 to over 3% per year by age 70. Model diagnostics showed that the log transformation ensured residual normality and stabilized variance.

Cortical ($\beta = -1.91$, SE = 0.09) and caudate ($\beta = -2.86 \times 10^{-2}$, SE = 0.29 x 10^{-2}) volumes showed a linear decline with advancing age (p-FDR<0.001), with an annual reduction on the order of 0.3%.

Compared with women, men showed significantly lower normalized brain ($\beta = -1.98 \times 10^{1}$, SE = 0.37×10^{1}), cortical ($\beta = -1.77 \times 10^{1}$, SE = 0.25×10^{1}), thalamic ($\beta = -8.28 \times 10^{-1}$, SE = 1.32×10^{-1}), and caudate ($\beta = -4.20 \times 10^{-1}$, SE = 0.87×10^{-1}) volumes (all $p < 0.001$) as well as higher normalized lateral ventricle volume ($\beta = 4.80 \times 10^{-2}$, SE = 1.61×10^{-2}, $p = 0.003$). Men also showed a significantly steeper age-related decline in normalized brain volume ($\beta = -5.22 \times 10^{-1}$, SE = 2.49, $p = 0.036$).

Normalized ChP volume remained relatively stable until approximately 35 years of age and then increased nonlinearly (all p-FDR <0.002), with annualized growth rates rising from 0.24% at age 35 to over 0.7% in later decades.

Demographic, Clinical, and Brain Volumetric Features in Patients With MS

Within the MS cohort, scanner subcohorts did not differ in sex, age, disease duration, EDSS score, or phenotype distribution (all $p \geq 0.093$). HE-DMTs were more frequent in the Scanner 2 subcohort (eTable 1).

Among clinical MS phenotypes, patients with RRMS and SPMS were more frequently female than HCs ($p \leq 0.018$),

Table 1 Demographic and Clinical Features in HCs and Patients With MS

	HCs (n = 461)	All MS (n = 727)	*p* Value	RRMS (n = 477)	SPMS (n = 160)	PPMS (n = 90)	RRMS vs HC *p* Value	SPMS vs HC *p* Value	PPMS vs HC *p* Value	SPMS vs RRMS *p* Value	PPMS vs RRMS *p* Value	SPMS vs PPMS *p* Value	*p* Value[a]
Demographic variables													
Sex, n (%)			0.022[b]				**0.005**[b]	**0.018**[b]	**0.028**[b]	0.736[b]	**<0.001**[b]	**<0.001**[b]	**<0.001**
Male	210 (46)	281 (39)		173 (36)	55 (34)	53 (59)							
Female	251 (54)	446 (61)		304 (64)	105 (66)	37 (41)							
Age [y]													
Mean (SD)	41.9 (15.1)	42.6 (11.3)	0.373[c]	39.1 (10.4)	48.9 (9.1)	49.9 (10.5)	**<0.001**[c]	**<0.001**[c]	**<0.001**[c]	**<0.001**[c]	**<0.001**[c]	0.470[c]	**<0.001**
Range	18.1–69.8	18.1–69.7		18.1–69.8	27.3–69.5	24.4–69.8							
Clinical variables													
Disease duration [y]													
Median (IQR)	—	10.5 (3.9–17.7)	—	8.0 (2.1–15.0)	18.9 (13.5–24.8)	9.5 (5.0–15.3)	—	—	—	**<0.001**[d]	**0.014**[d]	**<0.001**[d]	**<0.001**
EDSS score													
Median (IQR)	—	2.5 (1.5–5.0)	—	1.5 (1.0–2.5)	6.0 (5.0–6.5)	6.0 (4.0–6.5)	—	—	—	**<0.001**[d]	**<0.001**[d]	0.100[d]	**<0.001**
DMT status, n (%)[e]													
None		137 (19)	—	57 (12)	33 (21)	47 (52)	—	—	—	**0.002**[b]	**<0.001**[b]	**<0.001**[b]	**<0.001**
ME-DMT	—	361 (50)		272 (57)	68 (42)	21 (23)							
HE-DMT		229 (31)		148 (31)	59 (37)	22 (25)							

Abbreviations: DMT = disease-modifying therapy; EDSS = Expanded Disability Status Scale; HCs = healthy controls; HE = high-efficacy; IQR = interquartile range; ME = moderate-efficacy; MS = multiple sclerosis; PPMS = primary progressive multiple sclerosis; RRMS = relapsing-remitting multiple sclerosis; SPMS = secondary progressive multiple sclerosis.
Statistically significant comparisons are shown in bold.
[a] Heterogeneity among MS clinical phenotypes assessed using the χ^2 test (sex, DMT status), linear models (age), and the Kruskal-Wallis test (disease duration, EDSS score).
[b] Chi-square test.
[c] Welch *t* test.
[d] Mann-Whitney *U* test.
[e] ME-DMT = azathioprine, dimethyl fumarate, glatiramer acetate, methotrexate, interferon beta 1a, methotrexate, or teriflunomide; HE-DMT = alemtuzumab, cyclophosphamide, cladribine, fingolimod, natalizumab, ocrelizumab, ofatumumab, rituximab, or siponimod.

whereas patients with PPMS were more frequently male (p = 0.028) (Table 1). Compared with HCs, patients with RRMS were younger ($p < 0.001$), whereas patients with SPMS and PPMS were older ($p < 0.001$).

Compared with HCs, patients with MS showed significantly higher normalized brain T2-hyperintense WM LV and lateral ventricle volume (all p-FDR <0.001, Table 3, eFigure 2). Normalized brain, cortical, thalamic, and caudate volumes were significantly lower in patients with MS compared with HCs (all p-FDR<0.001).

In the direct comparisons among MS clinical phenotypes, both SPMS and PPMS cohorts were significantly older ($p < 0.001$), had a longer disease duration ($p \leq 0.014$), had higher EDSS scores ($p < 0.001$), and were more frequently untreated ($p \leq 0.002$) compared with patients with RRMS (Table 1). Patients with PPMS were also significantly more frequently male ($p = 0.028$).

Compared with patients with PPMS, those with SPMS were more frequently female ($p < 0.001$), had longer disease duration ($p \leq 0.014$), and were more frequently treated ($p \leq 0.002$) (Table 1). Compared with both RRMS and PPMS cohorts, patients with SPMS showed significantly higher normalized brain T2-hyperintense WM LV and lateral ventricle volumes (all p-FDR <0.001, Table 3, eFigure 2). They also had significantly lower normalized brain, cortical, thalamic, and caudate volumes (all p-FDR <0.001, Table 3, eFigure 2).

Table 2 Age-Related Trajectories and Slope Estimates for Normalized ChP and Normalized Global and Regional Brain Volumes in HC

	NChPV				NLVV				NBV			
Age [y]	EM (95% CI) [mL]	Slope CI [$\times 10^{-3}$]	p (p-FDR)	APVC [%]	EM (95% CI) [mL]	ES (SE) [$\times 10^{-3}$][a]	p (p-FDR)	APVC [%]	EM (95% CI) [mL]	ES (SE)	p (p-FDR)	APVC [%]
20	2.19 (2.10 to 2.29)	−11.5 to 5.3	0.450 (0.493)	—	17.0 (15.5 to 18.6)	−2.09 (2.13)	0.325 (0.374)	—	1,626 (1,617 to 1,635)	−0.84 (0.50)	0.095 (0.118)	—
25	2.18 (2.12 to 2.26)	−6.9 to 7.1	0.986 (0.986)	−0.07	16.7 (15.8 to 17.7)	−0.54 (1.71)	0.754 (0.788)	−0.30	1,621 (1,615 to 1,627)	−1.16 (0.40)	0.004 (0.005)	−0.06
30	2.19 (2.13 to 2.26)	−2.0 to 8.9	0.223 (0.270)	0.09	16.8 (16.0 to 17.6)	1.02 (1.30)	0.432 (0.485)	0.06	1,614 (1,610 to 1,619)	−1.47 (0.30)	**<0.001** (**<0.001**)	−0.08
35	2.22 (2.16 to 2.28)	2.8 to 10.7	**0.002** (**0.002**)	0.24	17.1 (16.3 to 18.0)	2.58 (0.92)	**0.005** (**0.007**)	0.42	1,606 (1,601 to 1,611)	−1.79 (0.21)	**<0.001** (**<0.001**)	−0.10
40	2.26 (2.20 to 2.33)	7.1 to 12.8	**<0.001** (**<0.001**)	0.38	17.8 (16.8 to 18.8)	4.14 (0.62)	**<0.001** (**<0.001**)	0.79	1,596 (1,591 to 1,602)	−2.11 (0.14)	**<0.001** (**<0.001**)	−0.12
45	2.32 (2.26 to 2.38)	10.1 to 15.5	**<0.001** (**<0.001**)	0.51	18.8 (17.8 to 20.0)	5.69 (0.56)	**<0.001** (**<0.001**)	1.16	1,585 (1,579 to 1,591)	−2.42 (0.13)	**<0.001** (**<0.001**)	−0.14
50	2.39 (2.33 to 2.45)	11.9 to 18.9	**<0.001** (**<0.001**)	0.61	20.3 (19.2 to 21.5)	7.25 (0.78)	**<0.001** (**<0.001**)	1.55	1,572 (1,566 to 1,578)	−2.74 (0.19)	**<0.001** (**<0.001**)	−0.16
55	2.47 (2.41 to 2.53)	12.9 to 21.9	**<0.001** (**<0.001**)	0.68	22.3 (21.1 to 23.5)	8.81 (1.14)	**<0.001** (**<0.001**)	1.94	1,558 (1,552 to 1,563)	−3.05 (0.28)	**<0.001** (**<0.001**)	−0.18
60	2.56 (2.50 to 2.63)	13.4 to 24.5	**<0.001** (**<0.001**)	0.73	24.9 (23.4 to 26.4)	10.37 (1.53)	**<0.001** (**<0.001**)	2.33	1,542 (1,535 to 1,548)	−3.37 (0.37)	**<0.001** (**<0.001**)	−0.21
65	2.66 (2.58 to 2.74)	13.2 to 26.3	**<0.001** (**<0.001**)	0.74	28.3 (26.0 to 30.7)	11.92 (1.95)	**<0.001** (**<0.001**)	2.74	1,524 (1,515 to 1,533)	−3.69 (0.47)	**<0.001** (**<0.001**)	−0.23
70	2.75 (2.66 to 2.86)	12.1 to 27.6	**<0.001** (**<0.001**)	0.72	32.7 (29.0 to 36.9)	13.48 (2.37)	**<0.001** (**<0.001**)	3.15	1,505 (1,492 to 1,518)	−4.00 (0.58)	**<0.001** (**<0.001**)	−0.25

	NCV				NTV				NCaV			
Age [y]	EM (95% CI) [mL]	ES (SE)	*p* (p-FDR)	APVC [%]	EM (95% CI) [mL]	ES (SE) [$\times 10^{-2}$]	*p* (p-FDR)	APVC [%]	EM (95% CI) [mL]	ES (SE) [$\times 10^{-2}$]	*p* (p-FDR)	APVC [%]
20	682 (678 to 686)	−1.91 (0.09)	**<0.001** (**<0.001**)	—	22.8 (22.5 to 23.1)	0.95 (1.77)	0.591 (0.633)	—	10.5 (10.3 to 10.6)	−2.86 (0.29)	**<0.001** (**<0.001**)	—
25	672 (669 to 676)			−0.28	22.8 (22.6 to 23.0)	−0.12 (1.41)	0.931 (0.952)	0.02	10.3 (10.2 to 10.4)			−0.27
30	663 (660 to 666)			−0.28	22.8 (22.6 to 22.9)	−1.19 (1.07)	0.266 (0.314)	−0.03	10.2 (10.1 to 10.3)			−0.28
35	653 (651 to 656)			−0.29	22.7 (22.5 to 22.9)	−2.27 (0.75)	**0.003** (**0.004**)	−0.08	10.0 (9.9 to 10.1)			−0.28
40	644 (641 to 646)			−0.29	22.5 (22.3 to 22.7)	−3.34 (0.51)	**<0.001** (**<0.001**)	−0.12	9.9 (9.8 to 10.0)			−0.28
45	634 (632 to 637)			−0.30	22.3 (22.1 to 22.5)	−4.41 (0.47)	**<0.001** (**<0.001**)	−0.17	9.8 (9.7 to 9.8)			−0.29
50	625 (622 to 628)			−0.30	22.1 (21.9 to 22.3)	−5.48 (0.68)	**<0.001** (**<0.001**)	−0.22	9.6 (9.5 to 9.7)			−0.29
55	615 (612 to 619)			−0.31	21.8 (21.6 to 22.0)	−6.55 (0.99)	**<0.001** (**<0.001**)	−0.27	9.5 (9.3 to 9.6)			−0.30
60	606 (601 to 610)			−0.31	21.4 (21.2 to 21.7)	−7.62 (1.32)	**<0.001** (**<0.001**)	−0.33	9.3 (9.2 to 9.5)			−0.30
65	596 (591 to 601)			−0.32	21.0 (20.7 to 21.3)	−8.70 (1.68)	**<0.001** (**<0.001**)	−0.38	9.2 (9.0 to 9.3)			−0.31
70	587 (581 to 592)			−0.32	20.6 (20.1 to 21.0)	−9.77 (2.03)	**<0.001** (**<0.001**)	−0.44	9.0 (8.9 to 9.2)			−0.31

Abbreviations: APVC = annualized percentage volume change; CI = confidence interval; EM = estimated mean; ES = estimated slope; FDR = false discovery rate; NBV = normalized brain volume; NCV = normalized cortical volume; NCaV = normalized caudate volume; NChPV = normalized choroid plexus volume; NLVV = normalized lateral ventricle volume; NTV = normalized thalamic volume; SE = standard error; y = years.
Mean estimated normalized global and regional brain volumes across ages (steps of 5 y) from sex and scanner-adjusted lifespan trajectories in HCs are reported. The first-order derivative (estimated slope) of the model is also shown to assess volume change rate. To aid interpretation, average annualized percentage volume changes over consecutive 5-y intervals computed from the corresponding estimated means are reported. By contrast, the NChPV lifespan trajectory was obtained using a two-step modeling framework, based on age-conditional estimated brain and lateral ventricle volumes, with 95% confidence intervals derived via bootstrap resampling (5,000 replicates) to account for propagated uncertainty. Slopes were consequently estimated numerically using finite differences rather than from model coefficients, and only bootstrap-based confidence intervals are reported. Analysis performed using robust linear regression models. FDR correction (Benjamini-Hochberg procedure) was applied to account for the overall number of tests.
Statistically significant comparisons are shown in bold.
[a] NLVV trajectory was modeled on the log scale. Estimated means and their 95% confidence intervals were back-transformed to the original scale for ease of interpretation. Estimated slopes and related standard error are reported on the log scale.

Compared with HCs, patients with MS showed enlarged ChP volume (estimated mean [EM] z-score = 0.452, p-FDR <0.001), consistently across MS phenotypes (EM z-score in RRMS = 0.442, SPMS = 0.515, PPMS = 0.400; heterogeneity-p = 0.744) (Table 3, eFigure 2).

Analysis of Associations in Patients With MS

Patients with MS exhibited significantly and uniformly higher normalized ChP volume z-scores than expected across the entire adult age spectrum (18–70 years) (all p-FDR<0.001), with no evidence of age-dependent variation (p = 0.957) (Table 4 and Figure 2).

Normalized ChP volume z-scores were already significantly increased as early as 1 year after clinical disease onset and were consistently higher across the subsequent 4 years (p-FDR = 0.012–0.015), after which they plateaued (Table 4 and Figure 2).

Although normalized ChP volume z-scores were not significantly associated across the full EDSS spectrum, when patients with MS were stratified based on an EDSS threshold of 3.0 (a cutoff between MS patients with mild disability and those with moderate or greater disability), higher normalized ChP volume z-scores were significantly associated with higher disability in MS patients with mild impairment (i.e., EDSS score <3.0) (β = 0.303, SE = 0.093, p = 0.001), but not in those with EDSS score ≥3.0 (β = −0.094, SE = 0.052 p = 0.070), and the interaction was significant (p < 0.001) (Figure 2).

Higher normalized ChP volume z-scores were also significantly associated with higher normalized T2-hyperintense WM LV (β = 0.012, SE = 0.004, p < 0.001) (Figure 2), whereas no significant associations with normalized brain, cortical, thalamic, caudate, or lateral ventricle volume z-scores were found (all p > 0.089).

No significant sex-related differences in normalized ChP volume z-scores were found (p = 0.275).

Associations Between ChP Volume and Immune-Related Genetic Scores in MS

A higher HLAGB score was significantly associated with higher normalized ChP volume z-scores (standardized β = 0.097, SE = 0.047, p = 0.038). By contrast, no significant associations were found for non-HLA PRS1 (standardized β = 0.024, SE = 0.047, p = 0.609), PRS2 (standardized β = 0.063, SE = 0.047, p = 0.177), and PRS3 (standardized β = 0.055, SE = 0.047, p = 0.241).

Neither HLAGB nor non-HLA PRS1, PRS2, and PRS3 were associated with normalized T2-hyperintense WM LV and brain volumetric measures (p ≥ 0.231).

A sensitivity analysis exploring HLAGB and each non-HLA PRS in combination confirmed that higher normalized ChP volumes z-scores were significantly associated only with higher HLAGB scores (p ≤ 0.036), but not with non-HLA PRSs (p ≥ 0.159).

Extreme decile analysis further supported these findings. By stratifying patients with MS by deciles of the HLAGB score, patients with MS in the highest decile showed significantly larger normalized ChP volume z-scores than those in the lowest decile (estimated mean difference = 0.478, SE = 0.207, 95% CI = 0.071; 0.885, p = 0.022) (Figure 3). Conversely, no significant differences in normalized ChP volume z-scores were observed between the top and bottom deciles of any non-HLA PRS (p ≥ 0.089) (eFigure 3, A–C).

Among the 24 IMSGC identified loci evaluated in the study, none showed significant association with normalized ChP volume z-scores after FDR correction, including HLA-DRB1*15:01 (eTable 2).

Robustness Analysis of the ChP Volume Model

The combined HC-MS model retained the same predictors as the HC-only model, with MS status as an additional significant predictor. No interaction terms between MS status and other predictors were retained, suggesting consistent associations between predictors and normalized ChP volume across groups. Z-scores in patients with MS derived from the HC-based and combined-sample models, computed excluding the MS term to preserve normative comparability, showed excellent agreement (r = 0.996, p < 0.001), supporting model robustness and its applicability to the MS population.

Discussion

In this monocentric cross-sectional study, we defined normative lifespan trajectories of ChP volume in HCs and quantified MS-related deviations using model-derived z-scores, while assessing associations with clinical, MRI, and genetic features. Leveraging a large HC cohort aged 18–70 years, we showed that ChP volume follows a nonlinear

Figure 1 Lifespan Trajectories of Explored Brain Structure Volumes in HC

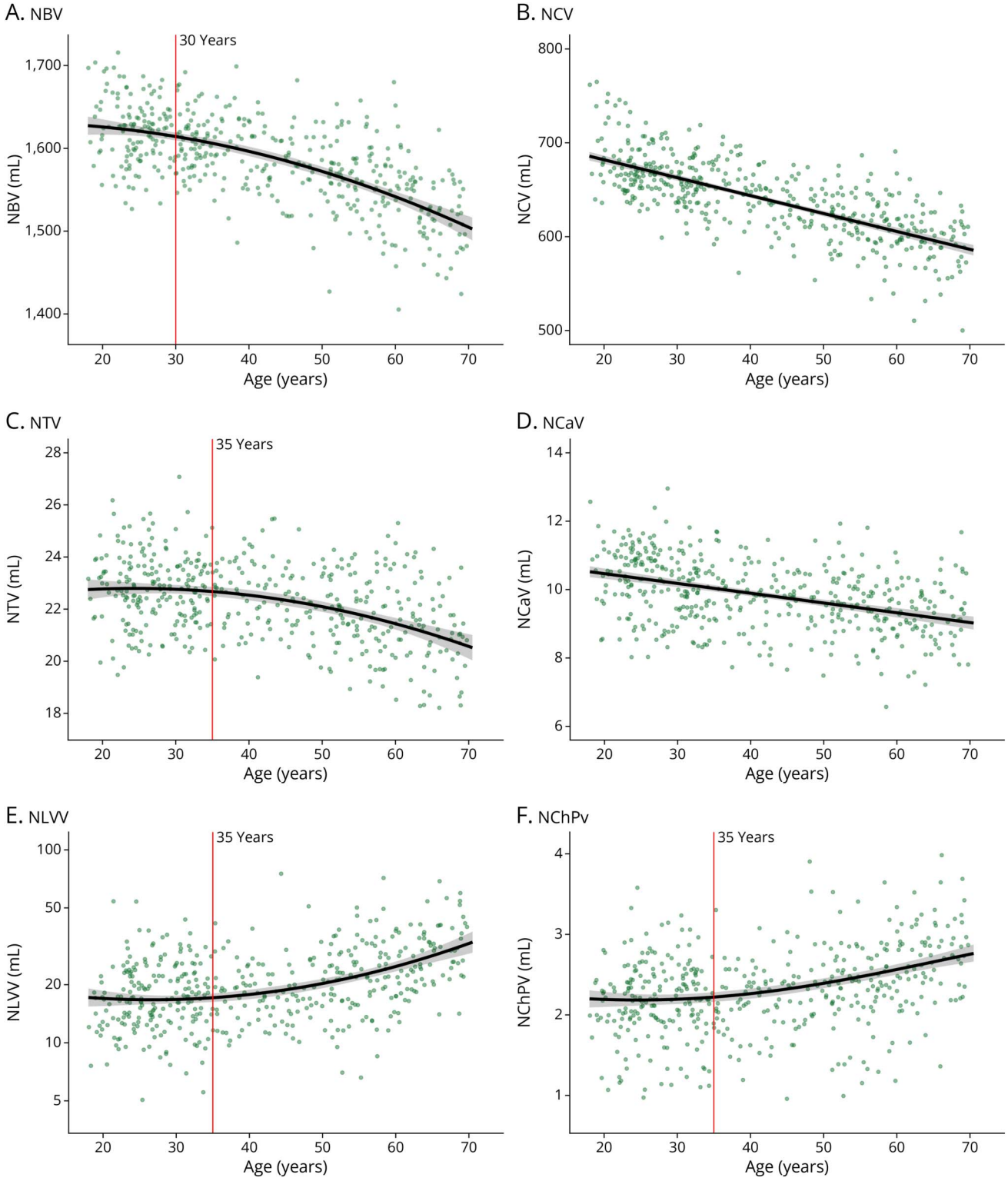

Age-related volume trajectories in HCs. (A) NBV and (C) NTV declined quadratically, with changes emerging around ages 30 and 35, respectively. (B) NCV and (D) NCaV declined linearly with age. (E) NLVV increased quadratically, with positive slopes evident from approximately age 35. (F) NChPV increased nonlinearly from around age 35. Gray-shaded areas represent the 95% confidence intervals around the estimated trajectories (text provides further details). HCs = healthy controls; NBV = normalized brain volume; NCV = normalized cortical volume; NCaV = normalized caudate volume; NChPV = normalized choroid plexus volume; NLVV = normalized lateral ventricle volume; NTV = normalized thalamic volume.

Table 3 Between-Group Comparisons of Normalized T2-Hyperintense WM LV and Brain Volumetric Z-Scores in Patients With MS

	MS (n = 727)		RRMS (n = 477)		SPMS (n = 160)		PPMS (n = 90)		SPMS vs RRMS	PPMS vs RRMS	SPMS vs PPMS	*p* Value[a]
	EM (SE) (95% CI)	*p* (*p*-FDR)	EM (SE) (95% CI)	*p* (*p*-FDR)	EM (SE) (95% CI)	*p* (*p*-FDR)	EM (SE) (95% CI)	*p* (*p*-FDR)	EMD (95% CI) *p* (*p*-FDR)	EMD (95% CI) *p* (*p*-FDR)	EMD (95% CI) *p* (*p*-FDR)	
NWM LV [ml][b]	5.061 (0.248) 4.575 to 5.547	**<0.001 (<0.001)**	4.133 (0.247) 3.649 to 4.617	**<0.001 (<0.001)**	10.187 (1.021) (8.186 to 12.187)	**<0.001 (<0.001)**	4.224 (0.559) (3.129 to 5.320)	**<0.001 (<0.001)**	6.054 (3.975 to 8.133) **<0.001 (<0.001)**	0.091 (−1.129 to 1.312) 0.883 (0.900)	5.962 (3.741 to 8.184) **<0.001 (<0.001)**	**<0.001**
NBV	−1.435 (0.067) −1.567 to −1.303	**<0.001 (<0.001)**	−1.171 (0.079) −1.326 to −1.017	**<0.001 (<0.001)**	−2.415 (0.137) −2.683 to −2.147	**<0.001 (<0.001)**	−1.139 (0.181) −1.495 to −0.784	**<0.001 (<0.001)**	−1.244 (−1.553 to −0.934) **<0.001 (<0.001)**	0.032 (−0.356 to 0.420) 0.872 (0.900)	−1.275 (−1.721 to −0.830) **<0.001 (<0.001)**	**<0.001**
NCV	−1.026 (0.059) −1.141 to −0.910	**<0.001 (<0.001)**	−0.884 (0.072) −1.025 to −0.744	**<0.001 (<0.001)**	−1.566 (0.125) −1.811 to −1.321	**<0.001 (<0.001)**	−0.849 (0.165) −1.174 to −0.524	**<0.001 (<0.001)**	−0.682 (−0.964 to −0.400) **<0.001 (<0.001)**	0.035 (−0.319 to 0.389) 0.844 (0.900)	−0.717 (−1.124 to −0.311) **<0.001 (<0.001)**	**<0.001**
NTV	−1.455 (0.059) −1.572 to −1.339	**<0.001 (<0.001)**	−1.224 (0.070) −1.362 to −1.086	**<0.001 (<0.001)**	−2.367 (0.123) −2.609 to −2.125	**<0.001 (<0.001)**	−1.223 (0.161) −1.538 to −0.907	**<0.001 (<0.001)**	−1.142 (−1.421 to −0.864) **<0.001 (<0.001)**	0.002 (−0.343 to 0.346) 0.992 (0.992)	−1.144 (−1.542 to −0.747) **<0.001 (<0.001)**	**<0.001**
NCaV	−0.729 (0.049) −0.825 to −0.634	**<0.001 (<0.001)**	−0.561 (0.058) −0.675 to −0.447	**<0.001 (<0.001)**	−1.346 (0.101) −1.543 to −1.148	**<0.001 (<0.001)**	−0.584 (0.133) −0.844 to −0.323	**<0.001 (<0.001)**	−0.784 (−1.012 to −0.556) **<0.001 (<0.001)**	−0.022 (−0.307 to 0.262) 0.877 (0.900)	−0.762 (−1.089 to −0.435) **<0.001 (<0.001)**	**<0.001**
NLVV	1.111 (0.048) 1.017 to 1.204	**<0.001 (<0.001)**	0.977 (0.057) 0.865 to 1.089	**<0.001 (<0.001)**	1.633 (0.099) 1.438 to 1.827	**<0.001 (<0.001)**	0.945 (0.132) 0.686 to 1.203	**<0.001 (<0.001)**	0.656 (0.431 to 0.881) **<0.001 (<0.001)**	−0.032 (−0.314 to 0.250) 0.823 (0.900)	−0.688 (−1.011 to −0.364) **<0.001 (<0.001)**	**<0.001**
NChPV	0.452 (0.046) 0.362 to 0.541	**<0.001 (<0.001)**	0.442 (0.056) 0.332 to 0.553	**<0.001 (<0.001)**	0.515 (0.099) 0.321 to 0.708	**<0.001 (<0.001)**	0.400 (0.131) 0.144 to 0.657	**0.002 (0.003)**	0.072 (−0.151 to 0.295) 0.524 (0.605)	−0.042 (−0.322 to 0.237) 0.767 (0.867)	0.115 (−0.207 to 0.436) 0.484 (0.572)	0.744

Abbreviations: CI = confidence interval; EM = estimated mean; EMD = estimated mean difference; FDR = false discovery rate; HCs = healthy controls; MD = mean difference; ml = milliliters; MS = multiple sclerosis; NBV = normalized brain volume; NCV = normalized cortical volume; NCaV = normalized caudate volume; NChPV = normalized choroid plexus volume; NLVV = normalized lateral ventricle volume; NTV = normalized thalamic volume; NWM LV = normalized white matter lesion volume; PPMS = primary progressive MS; RRMS = relapsing–remitting MS; SE = standard error; SPMS = secondary progressive MS.
Mean estimated z-scores, related SEs, 95% CIs, and *p* values testing the null hypothesis that mean z-score equals zero (i.e., healthy population expected value) in patients with MS, as a whole and according to their clinical phenotype. EMD, related 95% CI, and *p* values for between-group comparisons are also provided. Analyses were performed using robust linear regression models. Normalized brain T2-hyperintense WM LVs were compared using age, sex, and scanner-adjusted robust linear models. FDR correction (Benjamini-Hochberg procedure) was applied to account for the overall number of tests.
Statistically significant comparisons are shown in bold.
[a] Heterogeneity *p* values among MS clinical phenotypes.
[b] Analysis performed on log-transformed data. Estimated means, SEs, and 95% CI reported are back-transformed on the original scale using the delta method.

age-related pattern associated with global brain atrophy and ventricular enlargement, and that patients with MS exhibited early and consistently higher ChP volumes compared with HCs across ages and disease durations, linked to inflammatory lesion burden and HLA-mediated genetic burden.

In HCs, a model including age terms alone identified nonlinear, age-dependent ChP enlargement but explained only 16% of interindividual variance,[14,15] indicating that chronological age captures a limited component of ChP variability. To contextualize age-related ChP changes, we examined lifespan trajectories of other brain structures known to undergo physiologic aging. Normalized brain and thalamic volumes declined from age 30 to 35, paralleling ventricular expansion and linear caudate and cortical volume loss.[31-33] Adding brain and ventricular volumes increased explanatory power to 54%, indicating that a substantial proportion of ChP variability reflects underlying anatomical scaling. In the final model, normalized brain volume was negatively associated with ChP volume, while log-transformed normalized lateral

Table 4 Trajectories and Slope Estimates for Normalized ChP Volume Z-Score Over Age and Disease Duration in Patients With MS

	NChPV								
Age [y]	EM (95% CI)	*p* (*p*-FDR)	ES (SE) [$\times 10^{-2}$]	*p* Value	Disease duration [y]	EM (95% CI)	*p* (*p*-FDR)	ES (SE)[a]	*p* (*p*-FDR)
20	0.445 (0.261 to 0.629)	**<0.001 (<0.001)**	0.02 (0.40)	0.957	0	−0.007 (−0.290 to 0.276)	0.961 (0.961)	29.83 (10.50)	**0.005 (0.015)**
25	0.446 (0.295 to 0.596)	**<0.001 (<0.001)**			1	0.252 (0.105 to 0.399)	**<0.001 (0.001)**	21.94 (7.22)	**0.002 (0.012)**
30	0.447 (0.325 to 0.568)	**<0.001 (<0.001)**			5	0.463 (0.352 to 0.574)	**<0.001 (<0.001)**	12.19 (3.80)	**0.001 (0.012)**
35	0.448 (0.348 to 0.547)	**<0.001 (<0.001)**			10	0.542 (0.427 to 0.656)	**<0.001 (<0.001)**	4.88 (3.31)	0.141 (0.235)
40	0.449 (0.359 to 0.539)	**<0.001 (<0.001)**			15	0.556 (0.439 to 0.674)	**<0.001 (<0.001)**	−0.73 (4.76)	0.878 (0.878)
45	0.450 (0.353 to 0.547)	**<0.001 (<0.001)**			20	0.538 (0.399 to 0.677)	**<0.001 (<0.001)**	−5.46 (6.50)	0.402 (0.446)
50	0.451 (0.333 to 0.569)	**<0.001 (<0.001)**			25	0.498 (0.312 to 0.684)	**<0.001 (<0.001)**	−9.62 (8.18)	0.240 (0.300)
55	0.452 (0.305 to 0.599)	**<0.001 (<0.001)**			30	0.443 (0.191 to 0.696)	**<0.001 (<0.001)**	−13.38 (9.75)	0.170 (0.243)
60	0.453 (0.274 to 0.633)	**<0.001 (<0.001)**			35	0.377 (0.046 to 0.708)	**0.026 (0.032)**	−16.85 (11.22)	0.134 (0.235)
65	0.454 (0.240 to 0.669)	**<0.001 (<0.001)**			40	0.302 (−0.117 to 0.720)	0.158 (0.175)	−20.07 (12.61)	0.112 (0.235)
70	0.455 (0.205 to 0.706)	**<0.001 (<0.001)**							

Abbreviations: CI = confidence interval; EM = estimated mean; ES = estimated slope; FDR = false discovery rate; NChPV = normalized choroid plexus volume; SE = standard error.
Mean estimated NChPV z-scores across ages and disease duration at prespecified time points. The first-order derivative (estimated slope) of the model is also shown to assess z-score change rate. Analysis performed using robust linear regression models. FDR correction (Benjamini-Hochberg procedure) was applied to account for the overall number of tests. Statistically significant results are shown in bold.
[a] Estimated slopes and related standard error are reported with respect to square root–transformed DD. This transformation was applied to emphasize early-phase dynamics.

ventricle volume and its squared term captured a concave relationship, with ChP volume increasing at smaller ventricular sizes and slowing at larger volumes, reflecting the combined influence of brain atrophy and ventricular enlargement on ChP morphometry. Age was no longer independently associated with ChP volume after inclusion of volumetric measures, indicating that ChP volume primarily reflects global brain and ventricular anatomy rather than chronological aging.

Using this model, ChP volume in HCs remained stable until the mid-thirties and then increased nonlinearly. ChP enlargement with aging has been described previously[14,15,34] and aligns with histopathologic and imaging evidence of epithelial atrophy, basement membrane thickening, stromal fibrosis, calcifications, psammoma bodies, and ChP cysts,[15,35] as well as reduced ChP perfusion, possibly implicating altered CSF secretion and barrier functions.[14,15,36,37]

Applying the normative model to MS, ChP volume was already significantly enlarged 1 year after clinical onset and showed consistently higher cross-sectional z-scores during the first 5 years of disease, after which z-scores plateaued while remaining significantly higher compared with HCs. This pattern is consistent with findings in radiologically isolated syndrome,[7] clinically isolated syndrome,[6] and pediatric MS[5] and in a longitudinal study reporting ChP enlargement during the first 12 years of disease, followed by volumetric stabilization.[17] Differences in duration of ChP enlargement across studies[17] likely reflect methodological heterogeneity and incomplete adjustment for physiologic age-related ChP enlargement. It is important to note that this apparent plateau does not indicate normalization because ChP volume remained significantly higher than in HCs across disease durations.

ChP enlargement was consistently observed across MS clinical phenotypes.[6,8-13] Notably, higher normalized ChP volume z-scores were present across the adult age range, with no disease-by-age interaction, indicating additive and independent effects of MS and aging on ChP volume. Although cross-sectional, this early ChP enlargement pattern is consistent with inflammatory

Figure 2 Normalized ChP Volume Z-Scores Associations With Demographic, Clinical, and MRI Measures

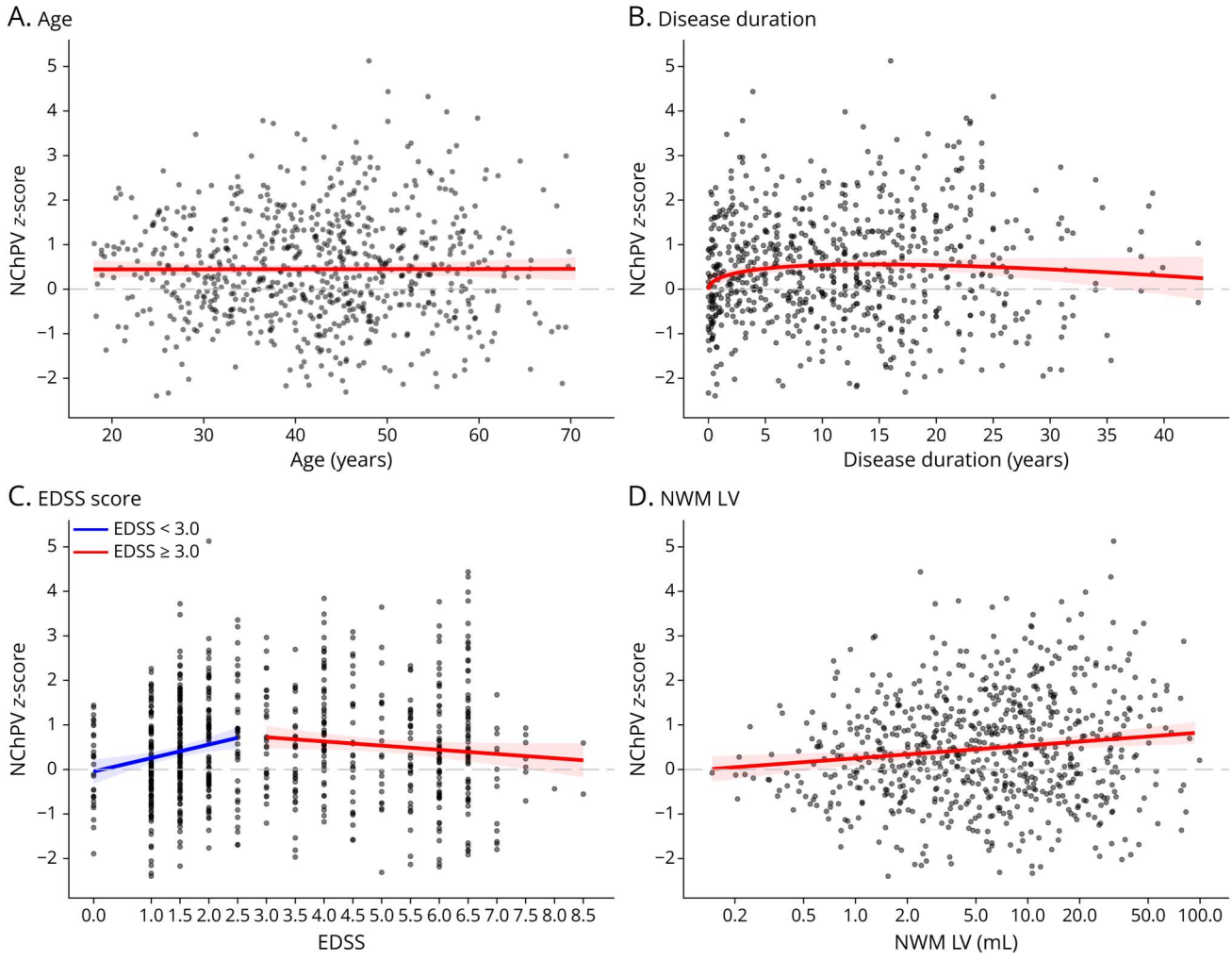

Scatterplots with fitted regression lines and 95% confidence intervals illustrate the relationships between NChPV z-scores and (A) age, (B) disease duration, (C) EDSS score, and (D) NWM LV. NChPV z-scores show no significant association with age but follow a nonlinear increase with disease duration, peaking around year 5. While no overall association is observed with EDSS scores, stratified analysis reveals a significant association in patients with MS with EDSS score <3.0 and no significant association in those with EDSS score ≥3.0. A positive association with NWM LV supports a link between ChP enlargement and inflammatory burden (text provides further details). ChP = choroid plexus; EDSS = Expanded Disability Status Score; MS = multiple sclerosis; NChPV = normalized choroid plexus volume; NWM LV = normalized white matter lesion volume.

activation at the BCSFB. In line with this hypothesis, preclinical models of experimental autoimmune encephalomyelitis showed immune cell accumulation in ChP before CNS infiltration, persisting during chronic disease.[4] MRI studies revealed associations of higher ChP volumes with gadolinium-enhancing lesions,[9] new WM lesion formation,[6] and relapse risk over up to 4 years.[9] Histopathologic correlates of MRI-detected ChP enlargement, particularly in early MS, remain limited, because most available human data derive from long-standing or progressive disease, underscoring the need for MRI-pathology studies exploring the substrates of early ChP changes. However, these early ChP modifications in MS may also reflect other mechanisms beyond focal inflammation, including intrinsic epithelial and stromal remodeling, altered vascular architecture and permeability, and dysregulated immune surveillance.[3,18,38-42] The apparent stabilization of ChP enlargement after the early disease phase may reflect a saturable inflammatory response and/or chronic remodeling processes (e.g., stromal fibrosis and extracellular matrix deposition),[3,18,38-42] limiting further expansion. In later phases, these ChP alterations may impair BCSFB integrity, CSF production, and glymphatic clearance.[39] Consistently, a reduction in the diffusion tensor imaging along the perivascular space index, a proposed marker of glymphatic function in vivo, occurs in the earliest phases of MS,[43,44] paralleling the early increase in ChP volume observed here and supporting a pathophysiologic interplay between ChP enlargement, CSF dynamics, and CNS damage.[43,44]

ChP z-scores correlated with EDSS scores only in mildly disabled patients, supporting an association with early disability-related inflammatory activity, but not in later phases dominated by neurodegeneration and compartmentalized

Figure 3 Distribution of Normalized ChP Volume Z-Scores in Patients With MS Stratified by Deciles of HLAGB Score

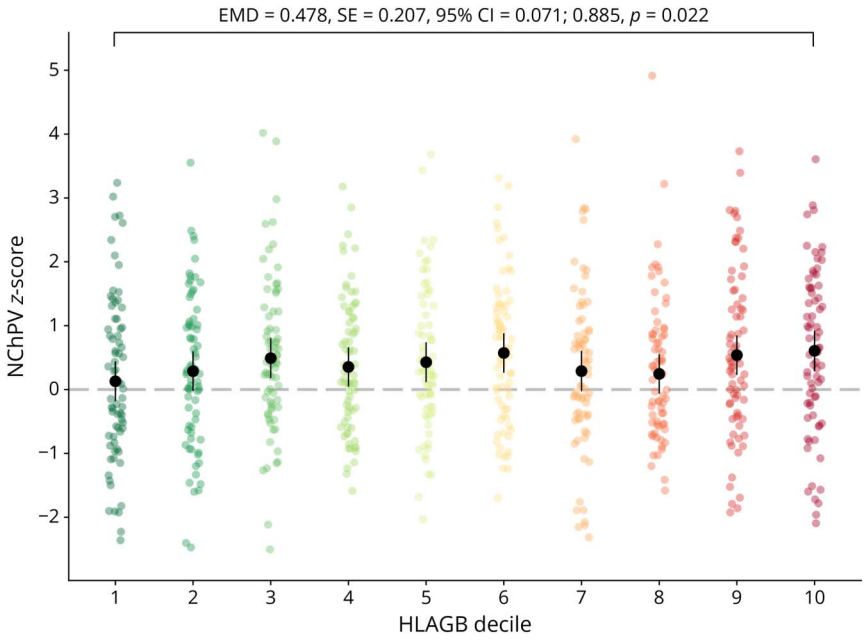

Dot-plot shows the distribution of NChPV z-scores across deciles of the HLAGB score, adjusted for age, sex, disease duration, EDSS, clinical phenotype, and DMT status, as well as the first 5 eigenvectors from population substructure PCA. Black dots and error bars represent the estimated means and 95% CI, respectively. The extreme decile comparison yielded a significant difference in NChPV z-scores only for HLAGB score, with higher values observed in patients within the highest HLAGB score decile compared with those in the lowest decile (p = 0.022, estimated mean difference = 0.478). ChP = choroid plexus; CI = confidence interval; DMT = disease-modifying therapy; EDSS = Expanded Disability Status Scale; EMD = estimated mean difference; HLAGB = human leukocyte antigen genetic burden; NChPV = normalized choroid plexus volume; PCA = principal component analysis; SE = standard error.

inflammation.[30,45,46] Clearly, given the cross-sectional design, this finding should not be interpreted as causal and may reflect co-correlating factors such as lesion burden, disease duration, treatment exposure, or other unmeasured confounders. ChP enlargement was significantly associated with higher normalized brain T2-hyperintense WM LV,[8,9] but not with cortical, thalamic, or caudate atrophy, supporting its role as an imaging correlate of focal inflammatory activity, distinct and temporally uncoupled from progressive neurodegeneration. Of note, after accounting for shared morphometric dependencies, residual ChP variability was more strongly related to inflammatory lesion burden than to global or regional brain volume loss, which may explain discrepancies with previous findings.[8,9,11]

Given the immunologic role of the ChP, we explored whether interindividual variability in immune-related genetic burden[23] was associated with ChP volumetric abnormalities in MS. Only higher HLAGB scores were significantly associated with higher normalized ChP volume z-scores, representing the sole significant association with MRI measures of structural brain damage. This specificity within the MS cohort aligns with HLA-mediated immune mechanisms in MS pathobiology[23,46] and with ChP immunologic functions.[1-3,38-40] The ChP contains antigen-presenting cells expressing MHC class II molecules[3,38,40]; moreover, it shows increased HLA-DR expression on epithelial and stromal cells[3] as well as transcriptomic upregulation of HLA-DRB1 and immune activation pathways in patients with MS compared with HCs.[38] Together, these findings suggest that cumulative HLA-associated genetic burden may enhance antigen-presenting capacity or proinflammatory signaling at the blood-CSF barrier, contributing to explain ChP enlargement in our cross-sectional analysis. Our results suggest that ChP enlargement correlates specifically with cumulative HLA burden rather than with any single variant, such as HLA-DRB1*15:01. While HLA-DRB1*15:01 represents the strongest individual genetic risk factor of MS,[23,24] this lack of association indicates that ChP enlargement is unlikely to be driven by a single-allele effect. Instead, it likely reflects broader polygenic immune dysregulation within the HLA locus. Given the complex linkage disequilibrium structure of the HLA region, multiple correlated variants acting on partially shared immune pathways may collectively modulate immune activation at the blood-CSF barrier, thereby contributing to interindividual variability in ChP enlargement. By contrast, the absence of associations with non-HLA PRSs supports specificity for HLA-mediated mechanisms.

Several limitations should be acknowledged. The cross-sectional nature of our data precludes causal inference regarding the temporal dynamics between ChP enlargement, disease onset, and progression. Longitudinal studies are necessary to determine whether baseline ChP volume predicts subsequent disease activity, disability progression, or treatment response. While we adjusted for key morphometric variables, our volumetric estimates were derived from 3D T1-weighted MRI, which may lack the resolution to accurately distinguish subtle anatomical subregions of the ChP or differentiate among epithelial hypertrophy, stromal expansion, and immune cell infiltration. Moreover, this sequence does not allow assessment of ChP microstructure, vascularity, or permeability. Although GM lesions may contribute to brain atrophy and ventricular enlargement, they were not

consistently evaluable in this retrospective cohort and could not be included as covariates. Multiparametric imaging approaches, including contrast-enhanced MRI and high-resolution or diffusion-based sequences, may enhance anatomical specificity and functional interpretation. Moreover, while our model adjusted for structural brain confounders, we did not assess potential modifiers such as systemic inflammation, metabolic status, hormonal fluctuations, or comorbidities. Because both DMT class and treatment duration may influence ChP volumetry, longitudinal studies with MRI acquired near treatment initiation and after defined periods of continuous therapy are needed to quantify within-participant ChP changes and to disentangle treatment effects from aging-related and disease stage–related variability. In this context, emerging evidence that high-efficacy DMTs may limit ChP enlargement compared with Me-DMTs[8] supports the potential role of ChP volumetry as a pharmacodynamic imaging marker. The absence of histopathologic validation or CSF biomarker data limits the interpretation of ChP enlargement as a direct marker of immune activity. Future studies integrating CSF cytokine profiles or pathologic ChP analyses will be essential to establish mechanistic correlations. The lack of genetic data in HCs prevented us from testing whether similar HLA effects occur outside the MS context, which should be addressed in future population-based imaging-genetic studies. Moreover, although the association between HLAGB and ChP volume was statistically robust, our HLA panel included only 24 of the 32 IMSGC-identified loci. This implies that other genetic, epigenetic, or environmental factors, including Epstein-Barr virus (EBV) exposure, smoking, vitamin D deficiency, and age at onset, likely modulate ChP structure and function.[25,38] For instance, previous MRI and serologic studies have shown associations between ChP enlargement and EBV serostatus, and recent evidence indicates that higher anti–EBNA-1 antibody titers are linked to greater ChP inflammatory changes in progressive MS,[47] supporting a potential immunopathogenic role of EBV at the CNS-immune interface. However, data regarding EBV serostatus were not available for our patient cohort. Moreover, future integrative multiomic studies are warranted to elucidate the complex interplay of genetic risk, immune regulation, and ChP remodeling. Finally, the absence of disease-control cohorts limits our ability to determine whether the observed ChP deviations are specific to MS or reflect broader mechanisms shared across neurologic diseases. However, this normative modeling framework provides a robust and generalizable tool for investigating ChP volumetric alterations in future studies evaluating other neurologic conditions (e.g., neuroinflammatory, neurodegenerative, or neuropsychiatric disorders), where ChP enlargement and dysfunction may contribute to disease pathophysiology.

In conclusion, we defined normative ChP volume trajectories in HCs and showed early ChP enlargement in MS, associated with inflammatory lesion burden, HLA-related genetic risk, and early disease duration and disability. Although blood-CSF barrier integrity was not directly assessed, our findings are consistent with ChP alterations reflecting inflammatory activity at brain border interfaces. Beyond pathogenic insights, ChP volumetry emerges as a promising noninvasive imaging correlate of immunogenetic burden and inflammatory processes in MS. Longitudinal studies in large, independent, and ideally multicentric cohorts with harmonized MRI protocols are warranted to confirm the sensitivity of ChP volumetry as a pharmacodynamic readout of DMT efficacy and CNS-specific anti-inflammatory mechanisms, to establish its clinical relevance across MS and other neuroinflammatory conditions, and to integrate barrier-sensitive MRI and CSF biomarkers to test whether ChP enlargement reflects measurable blood-CSF barrier dysfunction in vivo.

Author Contributions

P. Preziosa: drafting/revision of the manuscript for content, including medical writing for content; major role in the acquisition of data; study concept or design; analysis or interpretation of data. G. Corazzolla: drafting/revision of the manuscript for content, including medical writing for content; major role in the acquisition of data; study concept or design; analysis or interpretation of data. A. Meani: drafting/revision of the manuscript for content, including medical writing for content; analysis or interpretation of data. M. Margoni: drafting/revision of the manuscript for content, including medical writing for content; major role in the acquisition of data; analysis or interpretation of data. L. Storelli: drafting/revision of the manuscript for content, including medical writing for content; analysis or interpretation of data. E. Pagani: drafting/revision of the manuscript for content, including medical writing for content; analysis or interpretation of data. M. Rubin: drafting/revision of the manuscript for content, including medical writing for content; major role in the acquisition of data; analysis or interpretation of data. F. Clarelli: drafting/revision of the manuscript for content, including medical writing for content; analysis or interpretation of data. E. Mascia: drafting/revision of the manuscript for content, including medical writing for content; major role in the acquisition of data; analysis or interpretation of data. M. Sorosina: drafting/revision of the manuscript for content, including medical writing for content; major role in the acquisition of data; analysis or interpretation of data. F. Esposito: drafting/revision of the manuscript for content, including medical writing for content; major role in the acquisition of data; analysis or interpretation of data. M. Filippi: drafting/revision of the manuscript for content, including medical writing for content; study concept or design; analysis or interpretation of data. M.A. Rocca: drafting/revision of the manuscript for content, including medical writing for content; study concept or design; analysis or interpretation of data.

Study Funding

The authors report no targeted funding.

Disclosure

The authors declare that they have no competing interests in relation to this work. Potential conflicts of interest outside the

submitted work are as follows: P. Preziosa received speaker honoraria from Roche, Biogen, Novartis, Merck, Bristol Myers Squibb, Genzyme, Horizon, and Sanofi; he has received research support from the Italian Ministry of Health and Fondazione Italiana Sclerosi Multipla. G. Corazzolla, A. Meani, L. Storelli, E. Pagani, M. Rubin, F. Clarelli, E. Mascia, M. Sorosina, and F. Esposito have nothing to disclose. M. Margoni reports grants and personal fees from Sanofi Genzyme, Merck Serono, Roche, Biogen, Amgen, and Novartis. M. Filippi is Editor-in-Chief of the Journal of Neurology and Associate Editor of Human Brain Mapping, Neurological Sciences, and Radiology and received compensation for consulting services from Almirall, Biogen, Bristol-Myers Squibb, Eli Lilly, Merck, Novartis, Roche, and Sanofi; speaking activities from Amgen, Bayer, Biogen, Bristol-Myers Squibb, Celgene, Chiesi Italia SpA, Eisai, Eli Lilly, Fujirebio, Genzyme, Janssen, Merck, Neopharmed Gentili, Neuraxpharm, Novartis, Novo Nordisk, Roche, Sanofi, and Takeda; participation in Advisory Boards for Alexion, Biogen, Bristol-Myers Squibb, Eli Lilly, GE Healthcare Ltd, Merck, Neuraxpharm, Novartis, Roche, Sandoz, Sanofi, and Takeda; and scientific direction of educational events for Biogen, Merck, Roche, Celgene, Bristol-Myers Squibb, Lilly, Novartis, and Sanofi-Genzyme; he receives research support from Biogen Idec, Merck-Serono, Novartis, Roche, the Italian Ministry of Health, the Italian Ministry of University and Research, and Fondazione Italiana Sclerosi Multipla. M.A. Rocca received consulting fees from Biogen, Bristol Myers Squibb, and Roche and speaker honoraria from Alexion, Biogen, Bristol Myers Squibb, Celgene, Horizon Therapeutics Italy, Merck Serono SpA, Mitsubishi-Tanabe Pharma, Neuraxpharm, Novartis, Roche, Sandoz, and Sanofi. She receives research support from the MS Society of Canada, the Italian Ministry of Health, the Italian Ministry of University and Research, and Fondazione Italiana Sclerosi Multipla. She is Associate Editor for Multiple Sclerosis and Related Disorders and Associate Co-Editor for Europe and Africa for Multiple Sclerosis Journal. Go to Neurology.org/NN for full disclosures.

Publication History

Received by *Neurology® Neuroimmunology & Neuroinflammation* November 20, 2025. Accepted in final form March 17, 2026. Submitted and externally peer reviewed. The handling editor was Associate Editor Romana Höftberger, MD.

References

1. Proulx ST, Engelhardt B. Central nervous system zoning: how brain barriers establish subdivisions for CNS immune privilege and immune surveillance. *J Intern Med*. 2022; 292(1):47-67. doi:10.1111/joim.13469
2. Ghersi-Egea JF, Strazielle N, Catala M, Silva-Vargas V, Doetsch F, Engelhardt B. Molecular anatomy and functions of the choroidal blood-cerebrospinal fluid barrier in health and disease. *Acta Neuropathol*. 2018;135(3):337-361. doi:10.1007/s00401-018-1807-1
3. Vercellino M, Votta B, Condello C, et al. Involvement of the choroid plexus in multiple sclerosis autoimmune inflammation: a neuropathological study. *J Neuroimmunol*. 2008;199(1-2):133-141. doi:10.1016/j.jneuroim.2008.04.035
4. Lazarevic I, Soldati S, Mapunda JA, et al. The choroid plexus acts as an immune cell reservoir and brain entry site in experimental autoimmune encephalomyelitis. *Fluids Barriers CNS*. 2023;20(1):39. doi:10.1186/s12987-023-00441-4
5. Margoni M, Gueye M, Meani A, et al. Choroid plexus enlargement in paediatric multiple sclerosis: clinical relevance and effect of sex. *J Neurol Neurosurg Psychiatry*. 2023;94(3):181-188. doi:10.1136/jnnp-2022-330343
6. Klistorner S, Van der Walt A, Barnett MH, et al. Choroid plexus volume is enlarged in clinically isolated syndrome patients with optic neuritis. *Mult Scler*. 2023;29(4-5): 540-548. doi:10.1177/13524585231157206
7. Ricigliano VAG, Louapre C, Poirion E, et al. Imaging characteristics of choroid plexuses in presymptomatic multiple sclerosis: a retrospective study. *Neurol Neuroimmunol Neuroinflamm*. 2022;9(6):e200026. doi:10.1212/NXI.0000000000200026
8. Fleischer V, Gonzalez-Escamilla G, Ciolac D, et al. Translational value of choroid plexus imaging for tracking neuroinflammation in mice and humans. *Proc Natl Acad Sci USA*. 2021;118(36):e2025000118. doi:10.1073/pnas.2025000118
9. Ricigliano VAG, Morena E, Colombi A, et al. Choroid plexus enlargement in inflammatory multiple sclerosis: 3.0-T MRI and translocator protein PET evaluation. *Radiology*. 2021;301(1):166-177. doi:10.1148/radiol.2021204426
10. Muller J, Sinnecker T, Wendebourg MJ, et al. Choroid plexus volume in multiple sclerosis vs neuromyelitis optica spectrum disorder: a retrospective, cross-sectional analysis. *Neurol Neuroimmunol Neuroinflamm*. 2022;9(3):e1147. doi:10.1212/NXI.0000000000001147
11. Bergsland N, Dwyer MG, Jakimovski D, et al. Association of choroid plexus inflammation on MRI with clinical disability progression over 5 years in patients with multiple sclerosis. *Neurology*. 2023;100(9):e911-e920. doi:10.1212/WNL.0000000000201608
12. Preziosa P, Pagani E, Meani A, et al. Chronic active lesions and larger choroid plexus explain cognition and fatigue in multiple sclerosis. *Neurol Neuroimmunol Neuroinflamm*. 2024;11(2):e200205. doi:10.1212/NXI.0000000000200205
13. Rubin M, Preziosa P, Margoni M, et al. Dynamics of choroid plexus volume is associated with the presence and development of fatigue in multiple sclerosis. *J Neurol Neurosurg Psychiatry*. 2025;96(5):443-452. doi:10.1136/jnnp-2024-334913
14. Alisch JSR, Kiely M, Triebswetter C, et al. Characterization of age-related differences in the human choroid plexus volume, microstructural integrity, and blood perfusion using multiparameter magnetic resonance imaging. *Front Aging Neurosci*. 2021;13: 734992. doi:10.3389/fnagi.2021.734992
15. Sun Z, Li C, Zhang J, Wisniewski T, Ge Y. Choroid plexus aging: structural and vascular insights from the HCP-aging dataset. *Fluids Barriers CNS*. 2024;21(1):98. doi:10.1186/s12987-024-00603-y
16. Gueye M, Preziosa P, Ramirez GA, et al. Choroid plexus and perivascular space enlargement in neuropsychiatric systemic lupus erythematosus. *Mol Psychiatry*. 2024; 29(2):359-368. doi:10.1038/s41380-023-02332-4
17. De Meo E, Al-Araji S, Kanber B, et al. The temporal dynamics and clinical relevance of choroid plexus measures in multiple sclerosis. *Brain Commun*. 2025;7(3):fcaf239. doi: 10.1093/braincomms/fcaf239
18. Choi JD, Moon Y, Kim HJ, Yim Y, Lee S, Moon WJ. Choroid plexus volume and permeability at brain MRI within the Alzheimer disease clinical spectrum. *Radiology*. 2022;304(3):635-645. doi:10.1148/radiol.212400
19. Jeong SH, Park CJ, Cha J, et al. Choroid plexus volume, amyloid burden, and cognition in the Alzheimer's disease continuum. *Aging Dis*. 2024;16(1):552-564. doi: 10.14336/AD.2024.0118
20. Jeong SH, Park CJ, Jeong HJ, et al. Association of choroid plexus volume with motor symptoms and dopaminergic degeneration in Parkinson's disease. *J Neurol Neurosurg Psychiatry*. 2023;94(12):1047-1055. doi:10.1136/jnnp-2023-331170
21. Zhen Z, Zhang R, Gui L, et al. Choroid plexus cysts on 7T MRI: relationship to aging and neurodegenerative diseases. *Alzheimers Dement*. 2025;21(2):e14484. doi:10.1002/alz.14484
22. Serot JM, Foliguet B, Bene MC, Faure GC. Choroid plexus and ageing in rats: a morphometric and ultrastructural study. *Eur J Neurosci*. 2001;14(5):794-798. doi: 10.1046/j.0953-816x.2001.01693.x
23. International Multiple Sclerosis Genetics Consortium. Multiple sclerosis genomic map implicates peripheral immune cells and microglia in susceptibility. *Science*. 2019; 365(6460):eaav7188. doi:10.1126/science.aav7188
24. Sawcer S, Hellenthal G, Pirinen M, et al. International Multiple Sclerosis Genetics Consortium, Wellcome Trust Case Control Consortium 2. Genetic risk and a primary role for cell-mediated immune mechanisms in multiple sclerosis. *Nature*. 2011; 476(7359):214-219. doi:10.1038/nature10251.
25. Sorosina M, Esposito F, Guaschino C, et al. Inverse correlation of genetic risk score with age at onset in bout-onset and progressive-onset multiple sclerosis. *Mult Scler*. 2015;21(11):1463-1467. doi:10.1177/1352458514561910
26. Moutsianas L, Jostins L, Beecham AH, et al. Class II HLA interactions modulate genetic risk for multiple sclerosis. *Nat Genet*. 2015;47(10):1107-1113. doi:10.1038/ng.3395
27. Shams H, Shao X, Santaniello A, et al. Polygenic risk score association with multiple sclerosis susceptibility and phenotype in Europeans. *Brain*. 2023;146(2):645-656. doi: 10.1093/brain/awac092
28. Hilven K, Patsopoulos NA, Dubois B, Goris A. Burden of risk variants correlates with phenotype of multiple sclerosis. *Mult Scler*. 2015;21(13):1670-1680. doi:10.1177/1352458514568174
29. George MF, Briggs FB, Shao X, et al. Multiple sclerosis risk loci and disease severity in 7,125 individuals from 10 studies. *Neurol Genet*. 2016;2(4):e87. doi:10.1212/NXG.0000000000000087
30. Visani V, Veronese M, Pizzini FB, et al. ASCHOPLEX: a generalizable approach for the automatic segmentation of choroid plexus. *Comput Biol Med*. 2024;182:109164. doi:10.1016/j.compbiomed.2024.109164
31. Walhovd KB, Fjell AM, Reinvang I, et al. Effects of age on volumes of cortex, white matter and subcortical structures. *Neurobiol Aging*. 2005;26(9):1261-1278; discussion 1275-1268. doi:10.1016/j.neurobiolaging.2005.05.020
32. Dima D, Modabbernia A, Papachristou E, et al. Subcortical volumes across the lifespan: data from 18,605 healthy individuals aged 3-90 years. *Hum Brain Mapp*. 2022; 43(1):452-469. doi:10.1002/hbm.25320

33. Bethlehem RAI, Seidlitz J, White SR, et al. Brain charts for the human lifespan. *Nature*. 2022;604(7906):525-533. doi:10.1038/s41586-022-04554-y
34. Li Y, Zhou Y, Zhong W, et al. Choroid plexus enlargement exacerbates white matter hyperintensity growth through glymphatic impairment. *Ann Neurol*. 2023;94(1): 182-195. doi:10.1002/ana.26648
35. Praetorius J, Blazer-Yost B, Damkier H. *Role of the Choroid Plexus in Health and Disease, 1st 2020*. Springer; 2020.
36. Eisma JJ, McKnight CD, Hett K, et al. Choroid plexus perfusion and bulk cerebrospinal fluid flow across the adult lifespan. *J Cereb Blood Flow Metab*. 2023;43(2): 269-280. doi:10.1177/0271678X221129101
37. Bouzerar R, Chaarani B, Gondry-Jouet C, Zmudka J, Baledent O. Measurement of choroid plexus perfusion using dynamic susceptibility MR imaging: capillary permeability and age-related changes. *Neuroradiology*. 2013;55(12):1447-1454. doi: 10.1007/s00234-013-1290-2
38. Magliozzi R, Hametner S, Mastantuono M, et al. Neuropathological and cerebrospinal fluid correlates of choroid plexus inflammation in progressive multiple sclerosis. *Brain Pathol*. 2025;35(4):e13322. doi:10.1111/bpa.13322
39. Rodriguez-Lorenzo S, Ferreira Francisco DM, Vos R, et al. Altered secretory and neuroprotective function of the choroid plexus in progressive multiple sclerosis. *Acta Neuropathol Commun*. 2020;8(1):35. doi:10.1186/s40478-020-00903-y
40. Rodriguez-Lorenzo S, Konings J, van der Pol S, et al. Inflammation of the choroid plexus in progressive multiple sclerosis: accumulation of granulocytes and T cells. *Acta Neuropathol Commun*. 2020;8(1):9. doi:10.1186/s40478-020-0885-1
41. Prineas JW, Parratt JD, Kirwan PD. Fibrosis of the choroid plexus filtration membrane. *J Neuropathol Exp Neurol*. 2016;75(9):855-867. doi:10.1093/jnen/nlw061
42. Solar P, Zamani A, Kubickova L, Dubovy P, Joukal M. Choroid plexus and the blood-cerebrospinal fluid barrier in disease. *Fluids Barriers CNS*. 2020;17(1):35. doi: 10.1186/s12987-020-00196-2
43. Carotenuto A, Cacciaguerra L, Pagani E, Preziosa P, Filippi M, Rocca MA. Glymphatic system impairment in multiple sclerosis: relation with brain damage and disability. *Brain*. 2022;145(8):2785-2795. doi:10.1093/brain/awab454
44. Preziosa P, Pagani E, Margoni M, et al. Glymphatic system may mediate the relation between choroid plexus and brain damage in multiple sclerosis. *Neurol Neuroimmunol Neuroinflamm*. 2025;12(4):e200414. doi:10.1212/NXI.0000000000200414
45. Lublin FD, Haring DA, Ganjgahi H, et al. How patients with multiple sclerosis acquire disability. *Brain*. 2022;145(9):3147-3161. doi:10.1093/brain/awac016
46. Dendrou CA, Fugger L, Friese MA. Immunopathology of multiple sclerosis. *Nat Rev Immunol*. 2015;15(9):545-558. doi:10.1038/nri3871
47. Jakimovski D, Zivadinov R, Ramanathan M, et al. Greater humoral EBV response may be associated with choroid plexus inflammation in progressive MS. *J Neurovirol*. 2024; 30(5-6):545-549. doi:10.1007/s13365-024-01231-w